



## Far-Wake of a Sphere in a Stably Stratified Fluid: Characterization of the Vortex Structures

MARION BONNIER<sup>1,2</sup>, PHILIPPE BONNETON<sup>3</sup> and OLIVIER EIFF<sup>2</sup>

<sup>1</sup>Institut de Mécanique des Fluides de Toulouse, Allée du Pr. Camille Soula, 31400 Toulouse, France; <sup>2</sup>Centre National de Recherches Météorologiques, 42 Avenue G. Coriolis, 31057 Toulouse Cedex, France; <sup>3</sup>Département de Géologie et Océanographie, Université de Bordeaux, 1 Avenue des Facultés, 33405 Talence, France

**Abstract.** This article discusses the structure of the far-wake of a towed sphere in a saline stratification. We compare very low Froude number experiments to existing results at higher Froude numbers and investigate the vertical structure of the far-wake in terms of their vorticity and density fields. We show that the vertical propagation of vorticity is viscously dominated and propose a simple three-dimensional model for the quasi-equilibrium of the structure in terms of the density field.

**Key words:** stratified flow, quasi two-dimensional turbulence, far-wake dynamics, vorticity field, density measurements, vortex structure.

### 1. Introduction

The wake dynamics of a sphere in stratified flow raise a wide range of fundamental issues such as the collapse of three-dimensional turbulence, the resulting quasi two-dimensional turbulence or the emission of internal waves after the wake has developed and felt the constraint of stratification. These studies are of practical relevance for marine research and oceanographers since quasi two-dimensional motions contribute to deep-ocean dynamics.

Previous experimental studies of the horizontal and vertical expansion of the wake include those of Lin and Pao [10], Lin et al. [11] and Chomaz et al. [1]. These studies delineated the different flow regimes in terms of their Froude number ( $F$ ) and Reynolds number ( $Re$ ) dependence, and found that the Froude number appears to be the dominant control parameter.

For the turbulent regime ( $F = U/NR > 4.5$ , where  $U$  is the sphere velocity,  $N = -(g/\rho_0)/(\partial\rho/\partial z)^{1/2}$  is the Brunt–Väisälä frequency, and  $R$  is the radius of the sphere), one can easily distinguish two zones within the wake, namely the near-wake and the far-wake, since they are characterized by very different dynamics. Figures 1a and 1b show the far-wake and the near-wake, respectively, for the turbulent regime at  $F = 6$ . In the near-wake, for dimensionless times  $Nt < 2$ , the flow is independent of the stratification and evolves as it does in the

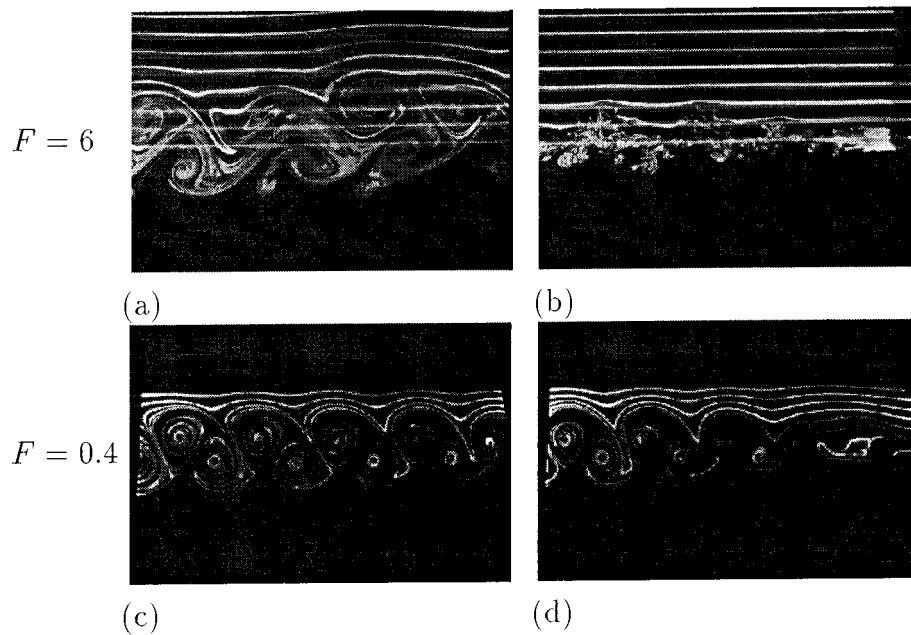


Figure 1. Comparison of the near and far-wakes for the laminar and turbulent regimes. The images are fluorescent-dye visualizations in the horizontal symmetry plane. (a)  $F = 6$ , far-wake; (b)  $F = 6$ , near-wake; (c)  $F = 0.4$ , far-wake; (d)  $F = 0.4$ , near-wake. The sphere moves from left to right.

homogeneous case, i.e., a three-dimensional spiral structure develops (Figure 1b). Eventually, the vortices in the near-wake start feeling the effect of the stratification, the turbulence collapses, loses its isotropy, and the turbulent wake becomes “quasi two-dimensional” in the form of a Kármán-like vortex street (Figure 1a). The turbulent far-wake is consequently defined as the region where the vertical components of velocity have become negligible compared to the horizontal ones. This generally occurs around  $Nt = 20$ . The turbulence is commonly referred to as being “quasi two-dimensional” in the sense that the vertical movements are negligible. The associated structures, on the other hand, are far from being uniform along the  $z$  (vertical) direction. Thus, as proposed by Godefert and Cambon [5], the term “quasi two-component” describes this flow more accurately since it implies that the  $w$  velocity-component (vertical) is negligible.

Figures 1c and 1d show the far-wake and near-wake, respectively, for the laminar regime at  $F = 0.4$ . For the laminar regime ( $F < 0.7$ ) the two zones are not easily distinguished. The fluid does not have enough potential energy to pass over the obstacle, and consequently a horizontal layer of fluid passes around the sphere and the wake immediately develops into a Kármán-like vortex street (Figure 1d) similar to what is observed in the turbulent far-wake (Figure 1a). It is strongly correlated along the vertical and can be characterized by a single layer.

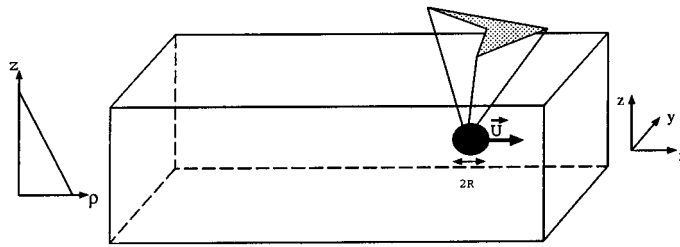


Figure 2. Schematic diagram of the experimental set-up. Tank dimensions are  $0.5 \times 0.5 \times 4 \text{ m}^3$  or  $0.8 \times 0.7 \times 7 \text{ m}^3$ . The typical linear saline stratification corresponds to a Brunt–Väisälä frequency close to one.

## 2. Experimental Set-Up and Techniques

The experiments were performed in two different towing tanks ( $0.5 \times 0.5 \times 4 \text{ m}^3$  and  $0.7 \times 0.8 \times 7 \text{ m}^3$ ) at the Centre National de Recherches Météorologiques of Météo France in Toulouse (Figure 2). The spheres are towed in a linear saline stratification of Brunt–Väisälä frequency ( $N$ ) close to one at  $F = 0.4$  ( $Re = 600$ ) and  $F = 6$  ( $Re = 1700$  or  $8000$ , depending on  $R$ ).

To visualize and study the flow in the far-wake of the sphere, two basic techniques were used: particle-tracking and fluorescent-dye visualization. In both techniques, a laser-sheet was used to vertically scan a succession of horizontal planes. These techniques will be referred to as the “fluorescence laser-sheet scanning technique” and the “particle laser-sheet scanning technique”. The planes of interest are filmed by CCD cameras and recorded on S-VHS tape for subsequent processing. To investigate the density variations within the flow, a fast-response micro-conductivity probe was used [6].

In the case of the fluorescence laser-sheet scanning technique, the dye was introduced into the flow by creating fixed vertical fluorescent-dye planes throughout the length of the tank (Figure 3). These planes were obtained by carefully pulling a vertical rake of thin cotton threads painted with fluorescent-dye shortly before towing the sphere. The planes appear as lines in any given horizontally-illuminated plane. Examples were presented earlier in Figures 1a–1d.

## 3. Far-Wake in the Horizontal Symmetry Plane

An extensive study of the far-wake has recently been conducted by Spedding et al. [12]. They used a particle image velocimetry (PIV) technique to study the wake for different regimes  $F \in [1.2; 7.9]$  on the isopycnal corresponding to a quasi-horizontal plane in the symmetry axis of the flow. The authors observed that a very high degree of coherence and organization is present in the far-wake in the form of periodic, alternating and counter-rotating quasi-circular, i.e., Kármán-like, vortex structures. They also observed that the turbulence statistics measured in the far-wake are characteristic of the power laws found in a homogeneous wake, which

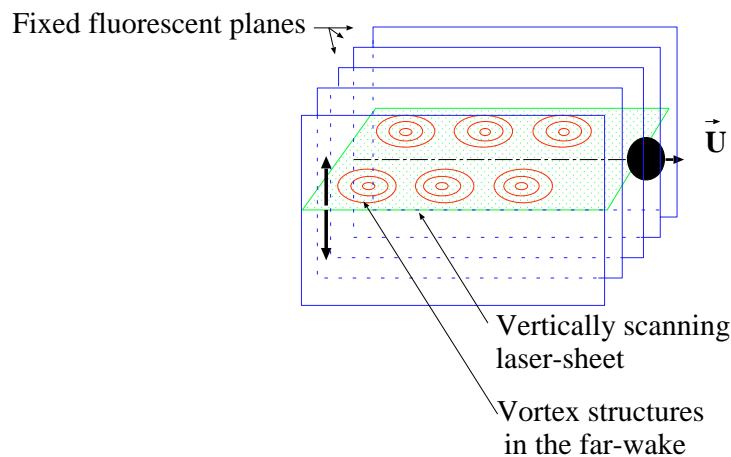


Figure 3. Vertical fluorescent planes are intersected by a horizontal laser-sheet scanning the vertical direction. This technique is referred to as the “fluorescence laser-sheet scanning technique”.

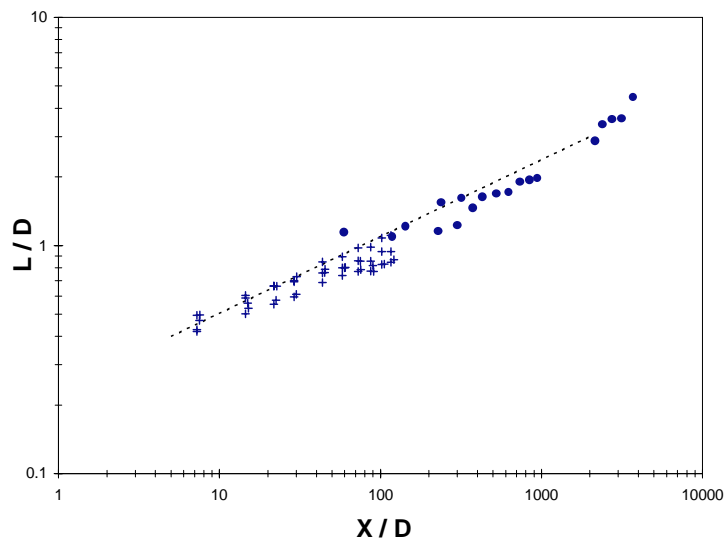


Figure 4. Lateral spreading of the two-dimensional vortex street. +,  $F = 0.4$ ; •,  $F = 6$ ; — — —, experimental curve-fit given by Spedding et al. [12] for  $F \in [1.2, 7.9]$ .

might be taken to imply that the far-wake turbulence is controlled by the near-wake turbulence. However, the earlier observation that different near-wake regimes lead to the same type of far-wake behavior, suggests that the far-wake behavior appears to be independent of the near-wake turbulence, at least within the range of Froude numbers investigated.

To pursue this issue a little further we have performed experiments at a lower Froude number than Spedding et al. [12], i.e., at  $F = 0.4$ , for which the near-

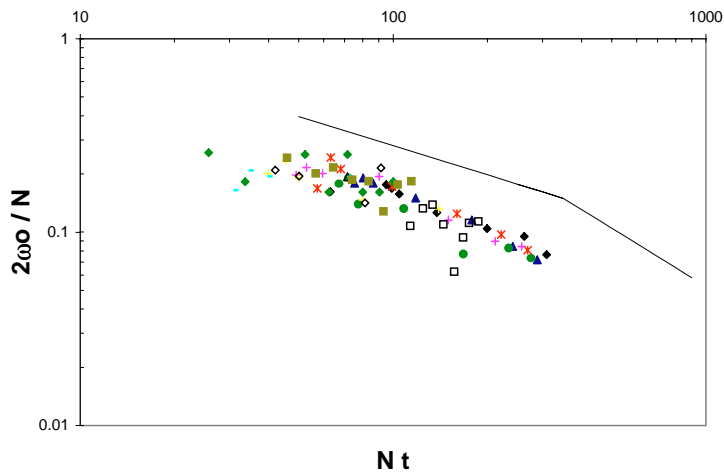


Figure 5. Decay of the peak vorticity in the horizontal symmetry plane for  $F = 0.4$ . —, curve fit to experimental results given by Spedding et al. [12] for  $F \in [1.2, 7.9]$ .

wake is laminar in nature, and compared them to the results of Spedding et al. [12]. Figure 4 shows the lateral spreading of the two-dimensional vortex street measured from our visualization experiments at  $F = 0.4$  (laminar) and  $F = 6$  (turbulent). Superimposed is the curve-fit given by Spedding et al. [12] for  $F \in [1.2, 7.9]$ . Figure 5 shows the decay of the peak vorticity for  $F = 0.4$  in the horizontal symmetry plane. Superimposed is a curve-fit to similar results given by Spedding et al. [12] for  $F \in [1.2, 7.9]$ . Even though the  $F = 0.4$  experiments correspond to a laminar near-wake, the quantities plotted in Figures 4 and 5 follow the same laws as found for the turbulent results of Spedding et al. [12]. This strengthens the view that the far-wake behavior is not necessarily controlled by the near-wake turbulence for the turbulent regimes.

Unfortunately, the observations discussed above do not provide clear evidence about the origin of the large-scale structures observed in far-wakes. Such structures are also known to exist in far-wakes of homogeneous flows, and two general views concerning their origin are commonly held. One is that the structures in the far-wake result from a hydrodynamic instability, i.e., after the initial turbulence has collapsed, the mean velocity profile destabilizes and new structures emerge in a disconnected fashion from those present in the near-wake (see, e.g., [2, 13]). The other view (see, e.g., [7, 8]) suggests that the far-wake structures evolve directly from the near-wake structures. Essentially, the same argument exists with respect to stratified flows, with Spedding et al. [12] holding the “evolution” view and Fung and Chang [4] the “instability” view. The observations made from Figures 4 and 5, although suggesting an independence of the far-wake behavior from the near-wake and thus reinforcing the instability argument, still do not rule out an evolutionary mechanism. They do suggest, however, that the characteristics of the laminar far-wake can be extrapolated to the turbulent regime, at least for the range investigated.

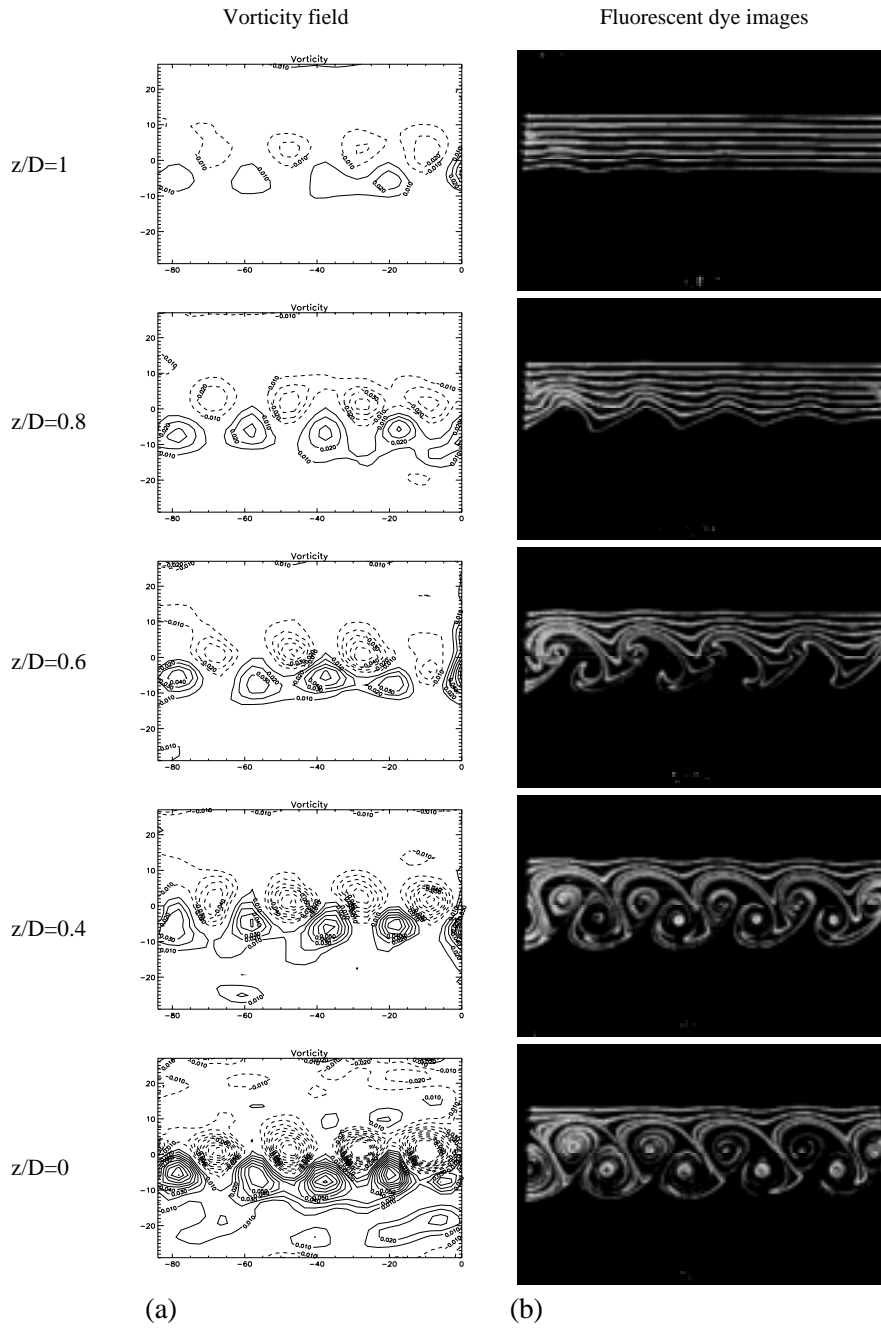


Figure 6. Horizontal planes at various  $z$ -levels for  $F = 0.4$  and  $Nt \sim 30$ . The sphere is moving from left to right. (a)  $\omega_z$ -vorticity isocontours obtained by the particle laser-sheet scanning technique; (b) fluorescent-dye images obtained by the fluorescence laser-sheet scanning technique.

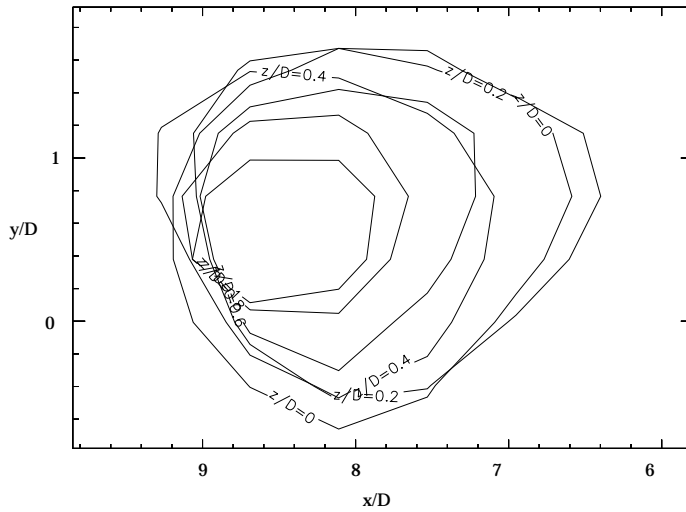


Figure 7. Superposition of a given vorticity isocontour ( $\omega = 0.2$  rad/s) of one vortex structure for five different  $z$ -levels with a total vertical span of  $z/D = 1$ . The sphere is moving from left to right. The dimensionless time is  $Nt \sim 100$ .

#### 4. Vertical Diffusion of the Horizontal Motions

To examine the vertical evolution of the horizontal motions we used both laser-sheet scanning techniques. Figure 6a shows the vertical vorticity isocontours computed from the particle tracking results at five horizontal slices with a total vertical span of  $z/D = 1$ , in the laminar far-wake ( $F = 0.4$ ). It can be seen from these results that the structures are organized in a Kármán-like fashion, up to  $z/D = 1$ . It should be emphasized that these slices are views of the *same* structures which are quasi-stationary in the time necessary to scan the flow ( $\Delta Nt = 20$ ). This implies that there is a high degree of vertical coherence. In order to better visualize the three-dimensional shape which is inherent to the various  $z$ -levels of the vorticity isocontours displayed in Figure 6a, we have superimposed vorticity isocontours of a particular value ( $\omega = 0.2$  rad/s) of one vortex structure at different  $z$ -levels. The result, shown in Figure 7 for  $Nt \sim 100$ , reveals that the inferred vortex lines starting from the symmetry plane are inclined in the opposite direction to the motion of the sphere. This inclination is likely due to the advection in the wake since it conforms with the shear direction. It should be noted that due to the finite time it takes to scan the flow, the inclination deduced from Figure 7 is in fact slightly underestimated.

To evaluate the vertical diffusion of the horizontal motions, it was more appropriate to use the fluorescence laser-sheet scanning technique. These experiments were conducted at  $F = 0.4$  and  $F = 6$ . A typical sequence of the horizontal planes obtained by vertically scanning the flow, from the symmetry plane up to one diameter above the symmetry plane, is shown in Figure 6b for  $F = 0.4$ . Using a constant threshold level to determine the perturbation induced by the vorticity field in the

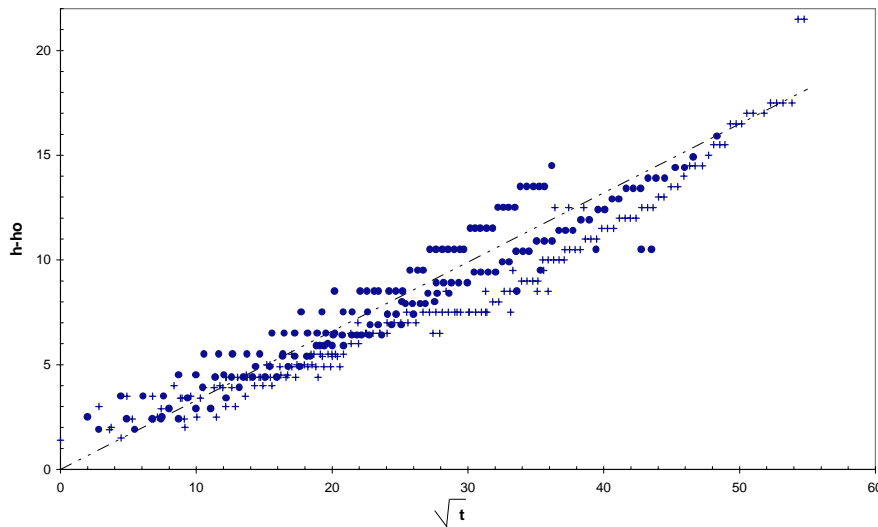


Figure 8. Vertical diffusion of the vorticity. +,  $F = 0.4$ ; •,  $F = 6$ ; - - - theoretical viscous diffusion law. The vorticity detection criteria is 6.5% of the peak vorticity measured in the horizontal symmetry plane. It should be noted that an increase in the dispersion of the data occurs when  $\sqrt{t} > 20$ . This is due to the onset of vortex pairing.

flow, we plotted the highest level perturbed against  $\sqrt{t}$ , since these two quantities should be proportional if the perturbation is due to viscous diffusion. From the results shown in Figure 8, it can be inferred that the vertical diffusion of the vortex street is indeed viscously dominated as the data follow a pure diffusion law based on the vorticity detection criteria. Although there has been some speculation [1] about other processes that could enhance the vertical transfer of vorticity, such as Eckman-like pumping and pumping due to centrifugal forces, our results do not support this, at least for the Froude and Reynolds numbers investigated. At very high Froude and Reynolds numbers, however, other processes cannot be excluded yet.

## 5. Density Structure of the Far-Wake

In order to assess the internal structure of the vortices revealed by the visualization results, we have performed conductivity measurements at  $F = 0.4$ . The conductivity probe was located behind the sphere at a fixed longitudinal distance equivalent to  $Nt = 20$ , with a lateral offset corresponding to the location of the vortex cores ( $\Delta y/D = 0.4$ ). Several  $z$ -levels above and below the wake axis were examined.

Figures 9a and 9b show typical density variations obtained from the conductivity measurements, above and below the wake axis. The distance between adjacent density peaks corresponds well with the observed vortex spacing in the flow visualization results. In addition to the inclination of the vortex lines previously discussed, these density signals display an asymmetry suggesting a distortion of the

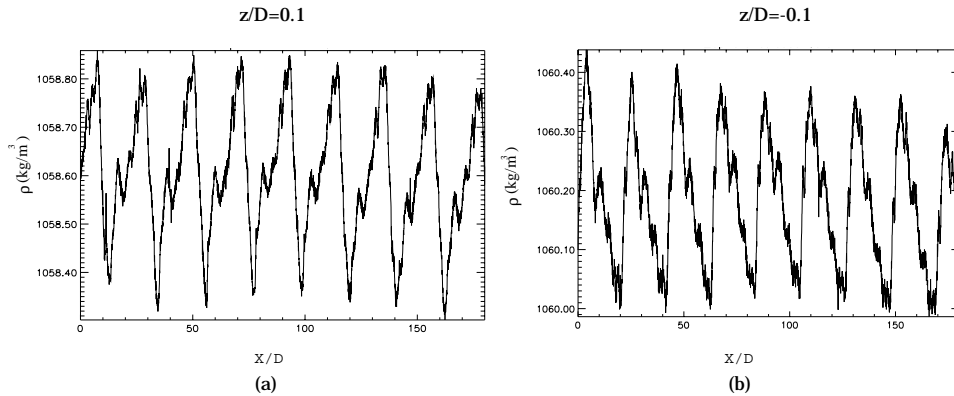


Figure 9. Density variations measured in the core of the vortices at  $F = 0.4$  and  $Nt = 20$ . (a)  $z/D = 0.1$  and (b)  $z/D = -0.1$  ( $X$  is in the reference frame of the tank).

density field within the vortices. Comparing similar density variations at various  $z$ -levels, it was observed that the peak-to-peak ( $\Delta\rho$ ) variations are very weak at the level of the sphere axis while the maxima occur *above* and *below* the symmetry plane. For  $|z/D| > 0.5$  no significant density variations were measured. From the peak-to-peak variations averaged over about 20 vortices traversed by the probe at several  $z$ -levels, we deduced the vertical  $\Delta\rho$ -profile of a single structure as shown in Figure 10. Although the measurements do not suggest the relative sign of  $\Delta\rho$  above and below the symmetry plane, the strong asymmetry of the recorded density signals suggests an opposite sign for  $\Delta\rho$  as sketched in Figure 10. This is in agreement with the three-dimensional model discussed in the next section.

The strong horizontal density variations displayed in Figures 9a and 9b are perhaps unexpected because we usually associate strong horizontal density variations with the presence of internal waves which are characterized by unsteady horizontal vorticity. In the case of the far-wake, however, the vorticity field is quasi-stationary with respect to the mean flow. The association of an unsteady horizontal component of vorticity with horizontal variations of density, can only be made, however, when the non-linear terms of the vorticity equation (Equation (1)) are ignored. According to Lighthill [9], the only manner to have a steady horizontal component of the vorticity (or by implication ultimate steady vortices), in Equation (1), is *not* to have any density variations along the horizontal direction – which of course is not satisfactory since it contradicts what has been observed in our experiments (e.g., Figures 9a and 9b). In order to explain the existence of both horizontal density variations and a steady horizontal component of vorticity, it is necessary to retain the non-linear terms of the vorticity equation. In that manner, quasi-stationary density variations result from a balance between the baroclinic term and the non-linear terms of the vorticity equation, and can account for steady horizontal vorticity (Equation (2)).

$$\frac{\partial \omega}{\partial t} = \frac{g}{\rho_0} \mathbf{e}_z \times \nabla \rho, \quad (1)$$

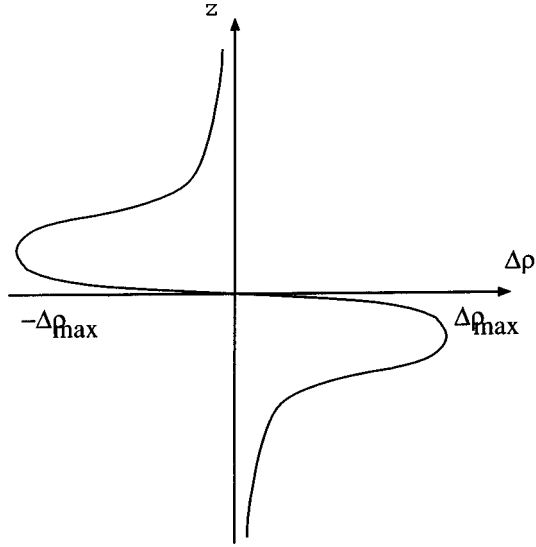


Figure 10. Sketch of an averaged peak-to-peak density variation profile within a single structure, as deduced from the density signals.

$$\frac{\partial \omega}{\partial t} = 0 = (\mathbf{u} \cdot \nabla) \omega - (\omega \cdot \nabla) \mathbf{u} - \frac{g}{\rho_0} \mathbf{e}_z \times \nabla \rho. \quad (2)$$

## 6. Equilibrium of a Single Vortex Structure

In this section we analyze a single vortex structure on the basis that the interactions between adjacent vortices in the far-wake are secondary compared to the dynamics within a given vortex. This seems a reasonable assumption when no vortex merging or other non-stationary interactions are observed.

To represent the observed vortex structure, we have chosen a steady axisymmetric velocity field (Equation (3)) from which we derived the density and pressure equations (Equation (4)) by resolving the stationary Boussinesq equations in polar coordinates. This represents a vortex of circular shape, with no singularity in its core and with vorticity distribution given by Equation (5). Except for the  $z$ -dependence, the vortex is comparable to the monopolar vortex studied by Flór et al. [3]. The velocity field is shown in Figure 11, and the computed density and pressure fields are shown in Figures 12a and 12b, respectively.

$$\begin{cases} u_r = 0 \\ u_\theta = \frac{Vr}{r_{\max}} \exp \frac{1}{2} \left( 1 - \frac{r^2 + z^2}{r_{\max}^2} \right) , \\ u_z = 0 \end{cases} \quad (3)$$

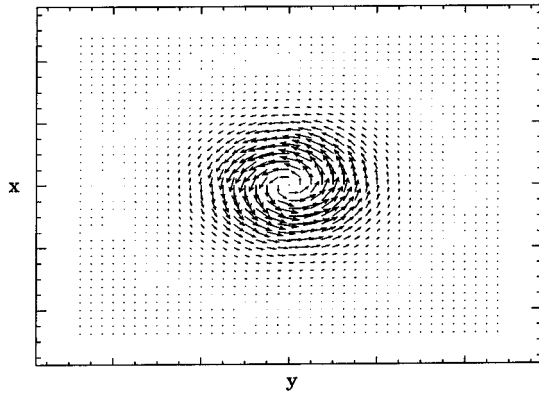


Figure 11. Example of the axisymmetric velocity field of the idealized vortex, visualized in a horizontal plane.

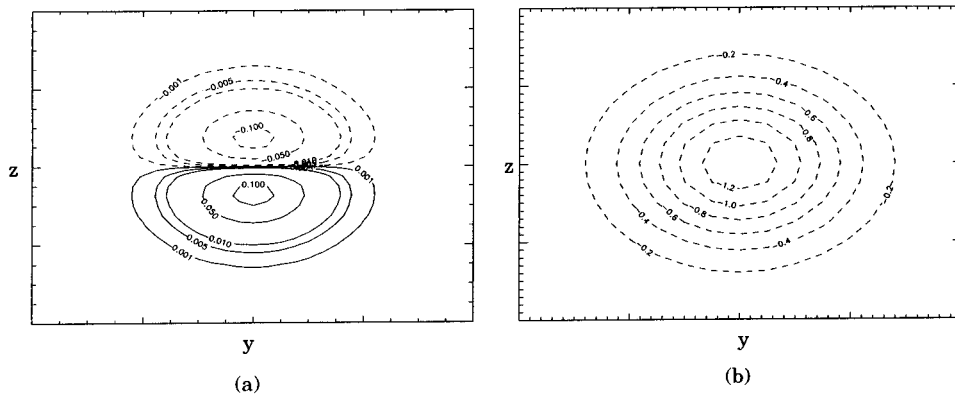


Figure 12. (a) Density field and (b) pressure field in a vertical plane of the idealized vortex structure. The dotted lines correspond to negative fluctuations.

$$\begin{cases} P(r, z) = -\frac{\rho V^2}{2} \exp\left(1 - \frac{r^2+z^2}{r_{\max}^2}\right) \\ \rho(r, z) = -\frac{\rho V^2}{g r_{\max}^2} z \exp\left(1 - \frac{r^2+z^2}{r_{\max}^2}\right) \end{cases}, \tag{4}$$

$$\begin{cases} \omega_r = \frac{V}{r_{\max}} \exp\left(\frac{1}{2}\left(1 - \frac{r^2+z^2}{r_{\max}^2}\right)\right) z \frac{r}{r_{\max}^2} \\ \omega_\theta = 0 \\ \omega_z = \frac{V}{r_{\max}} \exp\left(\frac{1}{2}\left(1 - \frac{r^2+z^2}{r_{\max}^2}\right)\right) \left(2 - \frac{r^2}{r_{\max}^2}\right) \end{cases}. \tag{5}$$

The idealized vortex structure presented here is in agreement with the density measurements discussed in Section 5. Specifically, the density isocontours shown in Figure 12a yield a vertical profile of the maximum density variations of the same shape as the one deduced from the measurements (Figure 10). Furthermore, a fixed probe passing through a succession of these idealized vortex structures would yield

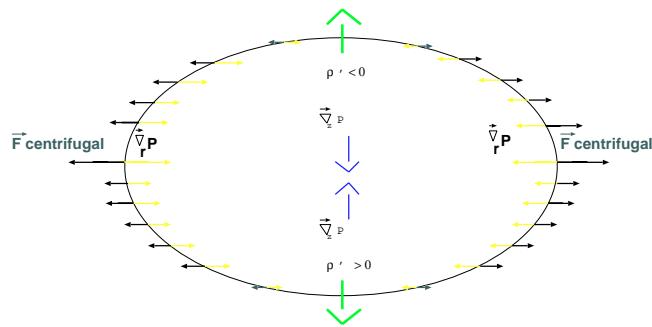


Figure 13. Three-dimensional balanced state in a vortex structure. In the horizontal direction, the horizontal pressure gradient is balanced by the centrifugal force whereas the vertical density gradient allows the hydrostatic balance.

the same type of horizontal density variations as those measured at several  $z$ -levels on both sides of the horizontal symmetry plane (Figures 9a and 9b). It should also be noted that this model is an example of a situation where horizontal density variations coexist with a steady horizontal component of vorticity.

It can be seen in Figure 12a that the density field of the vortex is divided into two parts: an upper part where the density is lighter than the ambient stratification and a lower part where it is heavier. The buoyancy forces due to this density field, acting on their own, would tend to expand the structure in the vertical direction. The lower pressure arising due to the centrifugal force in the vortex structure, however, has the balancing effect of contracting the structure in the vertical direction. In other words, it is possible to explain the observed quasi-stationarity of the vortex structures as a result of an adjustment between the centrifugal force and the pressure and density fields as illustrated in Figure 13.

## 7. Conclusion

A description of the vertical evolution within the far-wake was made using different complementary techniques. The results revealed a high degree of vertical coherence of the structures. These structures are, however, slightly inclined with respect to the vertical. It was also found that the vertical propagation of the vorticity is viscously dominated, at least for the laminar ( $F = 0.4$ ) and turbulent ( $F = 6$ ) cases investigated.

The conductivity measurements provided insight into the internal structure of the vortices for laminar far-wakes. The measurements showed strong horizontal density variations from which we were able to deduce the shape of the vertical density profile. A three-dimensional vortex model, similar to the two-dimensional monopolar vortex proposed by Flór and van Heijst [3], is shown to be consistent with the conductivity measurements. Thus, on the basis of this idealized vortex, the

quasi-equilibrium of the wake structures can be explained. Essentially, the three-dimensional density field adjusts to counter-balance the pressure field.

The characterization of the density structure is based on observations and measurements made at low Froude number, i.e., in a laminar far-wake. However, since the turbulent and laminar far-wakes were found to be similar, as discussed in Sections 3 and 4, it is not unlikely that the same kind of structures would be observed at the higher Froude number examined in the turbulent regime ( $F = 6$ ). Thus, the results are of interest for marine measurements because horizontal density variations should not only be associated to internal waves but can also be the signature of quasi two-dimensional vortices.

### Acknowledgements

This study was financially supported by the D.C.N. (Direction des Constructions Navales). All experiments were performed at the hydraulics laboratory of the Simulation Physique des Ecoulements Atmosphériques team at Météo-France.

### References

1. Chomaz, J.M., Bonneton, P., Butet, A. and Hopfinger, E.J., Vertical diffusion of the far wake of a sphere moving in a stratified fluid. *Phys. Fluids* **5**(11) (1993) 2799–2806.
2. Cimbala, J.M., Naghib, H.M. and Roshko, D.K., Large structure in the far wake of two-dimensional bluff bodies. *J. Fluid Mech.* **190** (1988) 265–298.
3. Flór, J.B. and van Heijst, G.J.F., Stable and unstable monopolar vortices in a stratified fluid. *J. Fluid Mech.* **311** (1996) 257–287.
4. Fung, Y.T. and Chang, S.W., Surface and internal wave signature of organized vortex motions in stratified fluids. *Phys. Fluids* **8**(11) (1996) 3023–3056.
5. Godeferd, F.S. and Cambon, C., Detailed investigation of energy transfers in homogeneous stratified turbulence. *Phys. Fluids* **6**(6) (1994) 2084–2100.
6. Head, M.J., The use of miniature four-electrode conductivity probes for high resolution measurements of turbulent density or temperature variations in salt-stratified water flows. Ph.D. Thesis, University of California, San Diego, CA (1983).
7. Huang, Z., Kawall, J.G. and Keffer, J.F., Development of structure within the turbulent wake of a porous body. Part 2. Evolution of the three-dimensional features. *J. Fluid Mech.* **329** (1996) 117–136.
8. Kopp, G.A. and Keffer, J.F., Coherent structures in two uniformly distorted plane turbulent wakes. *Phys. Fluids* **8**(10) (1996) 2706–2711.
9. Lighthill, J., Internal waves and related initial-value problems. *D.A.O.* **23** (1996) 3–17.
10. Lin, J.T. and Pao, Y.H., Wakes in stratified fluids. *Ann. Rev. Fluid Mech.* **11** (1979) 317–338.
11. Lin, Q., Lindberg, W.R., Boyer, D.L. and Fernando, H.J.S., Stratified flow past a sphere. *J. Fluid Mech.* **240** (1992) 315–354.
12. Spedding, G.R., Browand, F.K. and Fincham, A.M., Turbulence, similarity scaling and vortex geometry in the wake of a towed sphere in a stably stratified fluid. *J. Fluid Mech.* **314** (1996) 53–103.
13. Townsend, A.A., Flow patterns of large eddies in a wake and in a boundary layer. *J. Fluid Mech.* **95** (1979) 515–537.